









Lifetime measurement for the  $15/2_1^-$  and  $13/2_1^-$  levels in  $^{129}\text{Sn}$ D. Kumar <sup>1,2</sup>, A. Pal,<sup>1,2</sup> S. Basak <sup>1,2</sup>, T. Bhattacharjee <sup>1,2,\*</sup>, S. S. Alam,<sup>3</sup> L. Gerhard,<sup>4</sup> L. Knafla <sup>4</sup>, A. Esmaylzadeh <sup>4</sup>, M. Ley <sup>4</sup>, F. Dunkel,<sup>4</sup> K. Schomaker,<sup>4</sup> J.-M. Régis,<sup>4</sup> J. Jolie <sup>4</sup>, Y. H. Kim <sup>5,†</sup> and U. Köster<sup>5</sup><sup>1</sup>Variable Energy Cyclotron Centre, Kolkata 700 064, India<sup>2</sup>Homi Bhabha National Institute, Training School Complex, Anushakti Nagar, Mumbai 400 094, India<sup>3</sup>Government General Degree College, Chapra 741123, West Bengal, India<sup>4</sup>Institut für Kernphysik, Universität zu Köln, 50937 Köln, Germany<sup>5</sup>Institut Laue-Langevin, 38042 Grenoble, France

(Received 7 September 2023; revised 17 November 2023; accepted 19 January 2024; published 6 February 2024)

Lifetimes of the  $15/2_1^-$  and  $13/2_1^-$  levels in  $^{129}\text{Sn}$  have been measured using  $\gamma$ - $\gamma$  fast timing technique which come out to be 10(3) ps and 6(4) ps, respectively. The excited states were populated through internal transition decay of higher lying  $\mu\text{s}$  isomers in  $^{129}\text{Sn}$  produced as fission fragments and mass separated by the Lohengrin separator at Institut Laue-Langevin. The generalized centroid difference method was applied with four  $\text{LaBr}_3(\text{Ce})$  detectors, placed at the focal plane of the separator. The measured lifetimes and absolute transition probabilities are discussed in the light of large scale shell model calculations to interpret the single particle configurations and their mixing.

DOI: [10.1103/PhysRevC.109.024304](https://doi.org/10.1103/PhysRevC.109.024304)

## I. INTRODUCTION

The  $^{129}\text{Sn}$  nucleus, having three neutron holes in  $N = 82$  closed shell, provides information on the explicit role of neutron excitations around the double shell closure of  $^{132}\text{Sn}$ . Lifetime measurements in  $^{129}\text{Sn}$  are important to understand the nature of  $n - n$  interactions around this neutron-rich doubly-magic nucleus which has fundamental interest in both nuclear structure and nuclear astrophysics [1,2]. However, the lifetime data in odd- $A$  Sn nuclei around  $N = 82$  are scant and only available for very few levels.

The systematics of low lying energy states in odd- $A$  Sn isotopes reveals that, as one moves towards the  $N = 82$  shell closure, the  $\nu d_{3/2}$  and  $\nu h_{11/2}$  orbitals come closest to the Fermi surface. In  $^{129}\text{Sn}$ , the  $11/2^-$  state is observed at 35 keV above the  $3/2^+$  ground state and is, therefore, an isomer of 6.9 min. These two (almost degenerate) neutron orbitals play the most significant role in generating the excited configurations. The  $\nu s_{1/2}$  holes are also important for low lying excitations in odd- $A$  Sn as visible from the energy of the first  $1/2^+$  level in  $^{129}\text{Sn}$  that lies at 315 keV with a measured half-life of 19(10) ps [3].

The excitations built on the  $11/2^-$  level are the  $9/2^-$ ,  $7/2^-$ ,  $15/2^-$ , and  $13/2^-$  states which are systematically found in odd- $A$  Sn around  $N = 82$  [4,5]. Among these, the  $15/2^-$  and  $13/2^-$  levels are populated from the internal transition (IT) decay of the  $19/2^+$  isomers and decay directly to the  $11/2^-$  isomers, as shown in Fig. 1 of Sec. III (for  $^{129}\text{Sn}$ ). This set of

levels is interpreted to have  $\nu h_{11/2}^-$  types of structures with a variable admixture of other configurations [8] or the coupling of the  $\nu h_{11/2}$  orbital to the core  $2^+$  level. Lifetime measurements of  $15/2^-$  and  $13/2^-$  states may conclusively indicate the role of mixing of  $\nu h_{11/2}^-$ ,  $\nu d_{3/2}^-$ , and  $\nu s_{1/2}^-$  configurations in odd- $A$  Sn.

The low lying level structure of  $^{129}\text{Sn}$  is primarily known from  $\beta$  decay [6,7], isomer decay [8,9] and through relativistic fission and fragmentation reaction [10] studies. The information like spin parities of the excited levels and the multipolarities of the  $\gamma$  rays decaying from these levels are mostly adopted from systematics of experimental data and shell model interpretations in neighboring nuclei. Three long lived isomers in the  $\mu\text{s}$  range have been identified in  $^{129}\text{Sn}$  [7–10] above the  $11/2^-$  level following the decay curves of de-exciting  $\gamma$  transitions. However, there is no experimental data on the lifetime of other excited levels except that of  $1/2^+$  [3]. There are several theoretical calculations available, mostly based on a large scale shell model, to study the level structure and transition probabilities in  $^{129}\text{Sn}$  [3,11–13]. However, no calculation is available that shows the transition probabilities from the  $15/2^-$  and  $13/2^-$  levels excited on the  $11/2^-$  isomer.

In the present work, lifetimes of the  $15/2_1^-$  and the  $13/2_1^-$  states in  $^{129}\text{Sn}$  have been measured from isomeric decay.  $\gamma$ - $\gamma$  fast timing technique with a setup of four  $\text{LaBr}_3(\text{Ce})$  detectors, placed at the focal plane of the LOHENGRIN fission fragment separator at ILL, Grenoble, France, was used for this purpose. The transition probabilities have been estimated from the measured lifetimes; the single particle configurations and their mixing has been interpreted through comparison of experimental data with large scale shell model calculations.

\*Corresponding author: [btumpa@vecc.gov.in](mailto:btumpa@vecc.gov.in)

†Present address: Institute of Basic Science, Daejeon 34126, Republic of Korea.



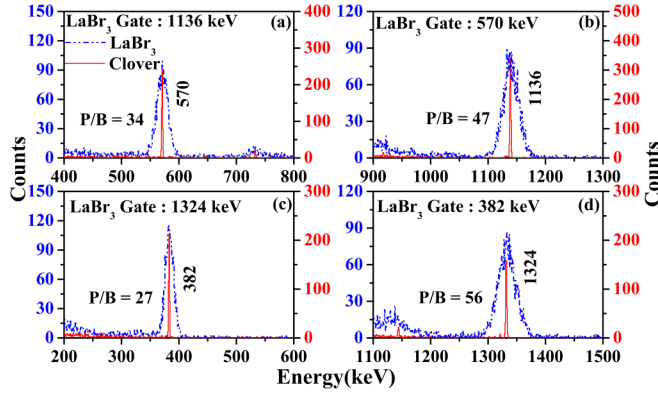


FIG. 2. The gated projections from IC gated  $\text{LaBr}_3$ - $\text{LaBr}_3$  and  $\text{LaBr}_3$ -clover coincidence events, corresponding to the cascades of  $15/2_1^-$  (a,b) and  $13/2_1^-$  (c,d) levels in  $^{129}\text{Sn}$ . The overlapped projections of  $\text{LaBr}_3$  and clover with a gate on  $\text{LaBr}_3$  show the cleanliness of a particular  $\gamma$  energy peak that may be used in subsequent lifetime measurement.

width at half-maximum (FWHM) of the energy peaks seen with  $\text{LaBr}_3$  detectors as visible from Figs. 1 and 2. Prompt three-fold coincidence events (IC- $\gamma$ - $\gamma$ ) gathered with any pair of  $\text{LaBr}_3$  detectors (two selected  $\gamma$  gates) and IC (with fragment gate) were considered for analysis. The delayed and antidelayed time difference distributions obtained for the cascades corresponding to  $15/2_1^-$  and  $13/2_1^-$  levels are shown in Fig. 3. In these figures, the FWHM of the distributions, representing the time resolution of the setup, is mentioned along with the total statistics obtained in these projections. The difference between the centroids of these distributions ( $\Delta C_{\text{exp}}$ ) generally contain the contributions from full energy peak (FEP)-Compton and Compton-Compton coincidences as well. Therefore, the same needs to be corrected to obtain the centroid difference corresponding to true FEP-FEP coincidences ( $\Delta C_{\text{FEP}}$ ). However, the gated projections of Fig. 2, corresponding to the  $\gamma$ - $\gamma$  cascades of  $15/2_1^-$  and  $13/2_1^-$  levels, show that the photopeaks are visible with peak to background ( $p/b$ ) ratios well above 20. Therefore, with such high  $p/b$ , the background corrections were negligibly small as compared to the error in lifetime, as also demonstrated in Ref. [14]. Accordingly, the experimental value of centroid differences shown in Fig. 3 ( $\Delta C_{\text{exp}}$ ) can be considered as  $\Delta C_{\text{FEP}}$  in the present measurement. The  $\Delta C_{\text{FEP}}$ , so measured, directly provides the measure of lifetimes of these levels, when corrected for the prompt response difference (PRD) of the setup following the relation  $2\tau = \Delta C_{\text{FEP}} - \text{PRD}$ .

The PRD curve for the present setup is discussed in detail in Ref. [15] and it represents the variation of time walk for the setup as a function of  $\gamma$  energy. As presented in Ref. [15], the PRD value over the total dynamic range of 40 keV to 1.4 MeV was less than 200 ps. In Fig. 3, the  $\Delta C_{\text{FEP}}$  ( $= \Delta C_{\text{exp}}$ ) and the PRD values for the cascades corresponding to  $15/2_1^-$  (a) and  $13/2_1^-$  (b) levels in  $^{129}\text{Sn}$  are shown which directly indicates the value of the lifetime ( $\tau$ ) of the levels. The lifetimes of the  $15/2_1^-$  and  $13/2_1^-$  levels, so measured in the present work, come out to be 10(3) ps and 6(4) ps, respectively. This is the first measurement for the lifetime of the  $15/2_1^-$  and  $13/2_1^-$  s

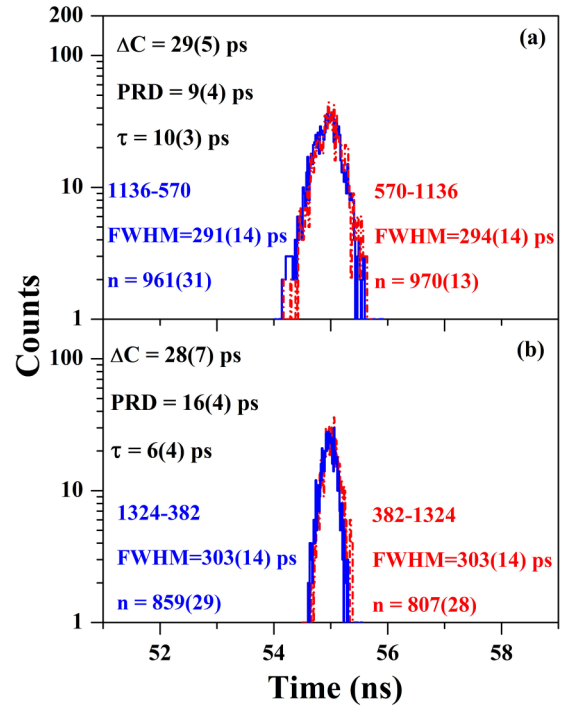


FIG. 3. The TAC projections for the lifetime measurements of  $15/2_1^-$  (a) and  $13/2_1^-$  (b) levels in  $^{129}\text{Sn}$ . The centroid difference ( $\Delta C = \Delta C_{\text{exp}} = \Delta C_{\text{FEP}}$ ) values are shown along with PRD values for the cascades. Lifetimes are also shown that are deduced following the relation  $2\tau = \Delta C_{\text{FEP}} - \text{PRD}$ . The FWHM values and the total counts obtained are mentioned for both delayed and antidelayed time difference distributions. See text for details.

levels in  $^{129}\text{Sn}$ . This also provides the first set of experimental data for the  $15/2_1^-$  and  $13/2_1^-$  levels among all odd- $A$  Sn and all  $N = 79$  nuclei around  $^{132}\text{Sn}$ . However, lifetime data are available in some Sn nuclei for the lowest  $1/2^+$  and other isomeric states like  $11/2^-$ ,  $19/2^+$ ,  $23/2^+$ , and  $27/2^-$ .

The reduced transition probabilities for the decay of  $15/2_1^-$  (1171.48 keV) and  $13/2_1^-$  (1359.40 keV) levels of  $^{129}\text{Sn}$  have been determined from the measured lifetimes. In this calculation, the consideration of the branching for the level decay as well as the mixing ratios and the conversion coefficients of 1136 keV and 1324 keV become important. Branching is reported as 100% for the decay of  $15/2_1^-$  and  $13/2_1^-$  levels of  $^{129}\text{Sn}$  [17].

The 1136 keV ( $15/2_1^- \rightarrow 11/2_1^-$ ) transition is expected to be pure  $E2$  in nature and therefore, it is reasonable to consider no mixing for the 1136 keV transition during calculation of the transition probability for the  $15/2_1^-$  (1171.48 keV) level.

The 1324 keV ( $13/2_1^- \rightarrow 11/2_1^-$ ) transition can be either pure  $M1$  or  $M1 + E2$  in nature. However, there is no experimental data on angular distribution and angular correlation for this transition which could indicate the mixing ratio. Due to lack of experimental information, pure  $M1$  nature has been considered for this transition. Therefore, the  $M1$  transition probability for the  $13/2_1^- \rightarrow 11/2_1^-$  decay has been deduced without any mixing and accordingly, provides the maximum possible value.

The conversion coefficients for the high energy E2 (1136 keV) and M1 (1324 keV) transitions were found to be very low (0.000977 and 0.000866, respectively) but were still considered in the calculation. The deduced values for the  $B(E2)(15/2_1^- \rightarrow 11/2_1^-)$  and  $B(M1)(13/2_1^- \rightarrow 11/2_1^-)$  rates in  $^{129}\text{Sn}$  were found to be 1.12(34) W.u. and 0.0023(15) W.u., respectively.

#### IV. SHELL MODEL CALCULATION

Large scale shell model calculations were performed to understand the underlying neutron configurations of the excited levels in  $^{129}\text{Sn}$  and the decay probabilities arising from the overlaps of their respective wave functions. In these calculations, performed with the NUSHELLX code [19], the neutron particles were distributed above the  $^{100}\text{Sn}$  core over 50–82 subshell space. The set of  $1g_{7/2}$ ,  $2d_{5/2}$ ,  $2d_{3/2}$ ,  $3s_{1/2}$ , and  $1h_{11/2}$  orbitals comprised the model space for both protons and neutrons. The  $sn100pn$  interaction [20] was used for the calculation without any truncation of the model space. The used interaction is well known and has been used in many nuclei of this mass region [15,22]. The results obtained on the excitation energy, single particle configurations, and the transition probabilities are discussed in the following subsections in comparison to the experimental data.

##### A. Excitation energy and single particle configuration

The low lying excitations in  $^{129}\text{Sn}$  including  $15/2^-$  and  $13/2^-$  levels could be well reproduced with the present calculation. The calculated level energies in comparison to experimental data are shown in Table I along with their single particle configurations. It is observed that the  $3/2_1^+$ ,  $11/2_1^-$ , and  $1/2_1^+$  levels are developed with the last odd hole in  $2d_{3/2}$ ,  $1h_{11/2}$ , and  $3s_{1/2}$  orbitals, respectively. The higher lying positive parity levels are also found to have mostly pure single particle configurations with very small mixing.

The configurations of the negative parity levels are fragmented based on the position of the neutron hole pairs distributed in all the other orbitals in the model space. It is observed that partition in the wave function is more prominent in case of  $11/2_1^-$  level and the maximum strength of the wave function for this level goes to  $\nu h_{11/2}^{-3}$  with considerable contribution from  $\nu s_{1/2}^{-2} h_{11/2}^{-1}$ . Major mixing of  $\nu d_{3/2}^{-2} h_{11/2}^{-1}$  and  $\nu s_{1/2}^{-1} d_{3/2}^{-1} h_{11/2}^{-1}$  configurations are also found in the wave functions of  $15/2_1^-$  and  $13/2_1^-$  levels which have significant strengths from  $\nu h_{11/2}^{-3}$  as well.

Shell model calculations have also been performed for  $2^+$  level in  $^{130}\text{Sn}$  and it is observed that the configuration of this level is an admixture of  $\nu h_{11/2}^{-2}$  (56%),  $\nu s_{1/2}^{-1} d_{3/2}^{-1}$  (19%), and  $\nu d_{3/2}^{-2}$  (11%). Therefore, the structure of  $15/2_1^-$  and  $13/2_1^-$  levels in  $^{129}\text{Sn}$  can also be understood in terms of coupling of one  $\nu h_{11/2}$  hole with the  $2^+$  level of  $^{130}\text{Sn}$  core.

##### B. Transition probability

The transition probabilities have been calculated with LSSM for the decay of  $15/2_1^-$  and  $13/2_1^-$  levels and also for

TABLE I. The level energies and single particle configurations for the low lying excitations in  $^{129}\text{Sn}$  calculated with NUSHELLX. The partitions having strength greater than 5% are shown.

$J^\pi$	Ex. energy		Configuration (SM)	
	Expt. (keV)	SM	Major partition	Strength (%)
$3/2_1^+$	0.0	0.0	$\nu(h_{11/2}^{-2}d_{3/2}^{-1})$	67
			$\nu(d_{3/2}^{-3})$	10
			$\nu(s_{1/2}^{-2}d_{3/2}^{-1})$	8
			$\nu(d_{3/2}^{-2}d_{3/2}^{-1})$	8
			$\nu(g_{7/2}^{-2}d_{3/2}^{-1})$	5
$11/2_1^-$	35.15	52	$\nu(h_{11/2}^{-3})$	39
			$\nu(d_{3/2}^{-2}h_{11/2}^{-1})$	34
			$\nu(s_{1/2}^{-2}h_{11/2}^{-1})$	11
			$\nu(d_{3/2}^{-2}h_{11/2}^{-1})$	8
			$\nu(g_{7/2}^{-2}h_{11/2}^{-1})$	6
$1/2_1^+$	315.41	289	$\nu(h_{11/2}^{-2}s_{1/2}^{-1})$	57
			$\nu(d_{3/2}^{-2}s_{1/2}^{-1})$	27
			$\nu(d_{5/2}^{-2}s_{1/2}^{-1})$	8
			$\nu(g_{7/2}^{-2}s_{1/2}^{-1})$	6
$15/2_1^-$	1171.48	1204	$\nu(d_{3/2}^{-1}s_{1/2}^{-1}h_{11/2}^{-1})$	34
			$\nu(d_{3/2}^{-2}h_{11/2}^{-1})$	25
			$\nu(h_{11/2}^{-3})$	21
			$\nu(d_{5/2}^{-1}s_{1/2}^{-1}h_{11/2}^{-1})$	7
			$\nu(g_{7/2}^{-1}d_{3/2}^{-1}h_{11/2}^{-1})$	7
$13/2_1^-$	1359.40	1586	$\nu(d_{3/2}^{-2}h_{11/2}^{-1})$	45
			$\nu(h_{11/2}^{-3})$	31
$15/2_1^+$	1741.89	1686	$\nu(d_{3/2}^{-1}s_{1/2}^{-1}h_{11/2}^{-1})$	11
			$\nu(h_{11/2}^{-2}d_{3/2}^{-1})$	82
$19/2_1^+$	1761.6	1705	$\nu(h_{11/2}^{-2}s_{1/2}^{-1})$	14
			$\nu(h_{11/2}^{-2}d_{3/2}^{-1})$	79
$23/2_1^+$	1802.6	1734	$\nu(h_{11/2}^{-2}s_{1/2}^{-1})$	17
			$\nu(h_{11/2}^{-2}d_{3/2}^{-1})$	97

the other levels for which lifetimes and transition probabilities are known either from theory or experiment. In Table II, the results from the present calculation have been shown in comparison to the experimental data obtained in the present work and also with those available in literature. It is observed that the effective charges and  $g$  factors play a significant role in the variation of  $B(E2)$  and  $B(M1)$  values, respectively, obtained in different calculations apart from the interactions used in the code.

The experimental data on transition probabilities for  $15/2_1^- \rightarrow 11/2_1^-$  and  $13/2_1^- \rightarrow 11/2_1^-$  decays, shown in Table II, have been obtained considering the transitions as pure  $E2$  and  $M1$ , respectively, as discussed in Sec. III. However, mixing of higher multipolarities may be possible in the case of  $13/2_1^- \rightarrow 11/2_1^-$  decay like this transition

TABLE II. The experimental and shell model (SM) results on the reduced transition probabilities for the decay of  $15/2_1^-$  and  $13/2_1^-$  levels of  $^{129}\text{Sn}$  are shown. The results for other levels are also included for which lifetimes were measured or calculated earlier. The  $J^\pi$  values have been taken from the ENSDF database [21].  $e_{\text{eff}}^\nu$  and  $g_s^\nu$  values are also included as these parameters are found to have significant effect on the calculated transition probabilities. Data from Ref. [13] have been extracted from the graph. See text for other relevant details.

$J_i^\pi \rightarrow J_f^\pi$	Mutipolarity	Transition probability(W.u.)			Reference
		Expt.	Theory	$e_{\text{eff}}^\nu$	
$(23/2_1^+) \rightarrow (19/2_1^+)$	$E2$	1.29(15) 1.24(10) 1.29(22)	$B(E2)$		
			1.93	0.86(8)	[7]
			0.62	0.9	[9]
			0.99	0.85	[10]
			0.63		[11]
			1.38	0.7	[12]
			1.47		[13]
			0.58	0.5	present work
			1.14	0.7	present work
			1.88	0.9	present work
$(19/2_1^+) \rightarrow (15/2_1^+)$	$E2$	1.32(18) 0.83(5) 1.37(7) 1.52(18)	$B(E2)$		
			2.84	0.69(10)	[7]
			1.45	0.9	[8]
			1.66	0.85	[9]
			1.39		[10]
			1.27	0.7	[11]
			1.03		[12]
			0.84	0.5	[13]
			1.65	0.7	present work
			3.14	0.9	present work
$(15/2_1^-) \rightarrow 11/2_1^-$	$E2$	1.12(34)	$B(E2)$		
			0.97	0.5	present work
			1.90	0.7	present work
			3.14	0.9	present work
			2.63		[13]
$(13/2_1^-) \rightarrow 11/2_1^-$	$M1$	0.0023(15)	$B(M1)$		
			0.0014	$g_s^\nu$	-3.82
$(1/2_1^+) \rightarrow 3/2_1^+$	$M1$	$3.6(19) \times 10^{-2}$	0.0007	-2.68	present work
			$3.24 \times 10^{-5}$	-2.68	[3]
			$3.0 \times 10^{-3a}$	-2.68	[3]
			$3.8 \times 10^{-4}$	-2.68	[12]
			$4.2 \times 10^{-5}$	-2.68	present work
	$8.6 \times 10^{-5}$	-3.82	present work		

<sup>a</sup>With modified M1 operator.

is known as  $M1 + E2$  in  $^{131}\text{Te}$  [18], the only information existing in this region. Such mixing in  $^{129}\text{Sn}$ , if any, may also be estimated from a shell model calculation which was found to be  $\delta = 1.07$ . The  $B(M1)$  and  $B(E2)$  values for this decay have, therefore, been calculated considering the mixing obtained from shell model and the measured lifetime. These values were found to be 0.0011(7) and 0.46(31), respectively.

It is found that a variety of effective charges have been used in the calculations of  $B(E2)$ s available in literature. In the present work also, the  $B(E2)$  rates have been calculated with variation of neutron effective charge  $e_{\text{eff}}^\nu$  from 0.5 to 0.9. It is found that the default values of  $e_{\text{eff}}^\nu = 0.5$  could better reproduce the experimental data for the  $15/2_1^-$  level although higher effective charges are required to explain the  $B(E2)$  data at higher spins. This corroborates with our earlier observation

in the case of the  $B(E2)$  values in Te and Xe nuclei around  $^{132}\text{Sn}$  [15,22] with few neutron holes. In these calculations, the default effective charges ( $e_{\text{eff}}^\pi = 1.5$ ,  $e_{\text{eff}}^\nu = 0.5$ ) could well reproduced the experimental data using  $sn100pn$  interaction.

For the calculation of  $B(M1)$  rates,  $g_s^\nu = -2.68$  has been used for the decay of the  $1/2_1^+$  level [3,12]. In the present work, the calculation has been performed with default values of  $g$  factors ( $g_l^\pi = 1.0$ ,  $g_s^\pi = 5.586$ ,  $g_l^\nu = 0.0$ , and  $g_s^\nu = -3.826$ ) and also modifying  $g_s^\nu$  to  $-2.68$ . In the present calculation, the  $B(M1)$  rate is reasonably reproduced for the  $13/2_1^-$  level with default  $g_s^\nu$ . This  $g_s^\nu = -3.82$  also provides a  $B(M1)(1/2_1^+ \rightarrow 3/2_1^+)$  which is closer to the experimental data compared to that obtained with  $g_s^\nu = -2.68$ . The  $B(M1)$  value obtained in the present work for the  $1/2_1^+$  level and with  $g_s^\nu = -2.68$ , however, corroborates well with the value calculated in Ref. [3] using the same  $g_s^\nu$ . However, it may

be noted that calculations, performed in Ref. [3], using  $g_s^v = -2.68$  and with modified  $M1$  operator only could obtain the  $B(M1)(1/2_1^+ \rightarrow 3/2_1^+)$  rate closest to the experimental data.

Specific to the negative parity levels, the experimental transition probabilities for the decay of  $15/2_1^-$  and  $13/2_1^-$  states could be reasonably reproduced from the shell model. This, in turn, validates the corresponding single particle configurations proposed for these two levels. Therefore, the presence of configuration mixing with the pure  $\nu h_{11/2}^-$  wave function is quantitatively confirmed for the  $15/2_1^-$  and  $13/2_1^-$  levels in  $^{129}\text{Sn}$ .

## V. SUMMARY

Lifetimes of the  $15/2_1^-$  and  $13/2_1^-$  levels in  $^{129}\text{Sn}$  have been measured using  $\gamma$ - $\gamma$  fast timing technique. The measured

lifetimes provide the first ever experimental data set for the  $15/2_1^-$  and  $13/2_1^-$  levels developed above  $11/2^-$  in odd- $A$  Sn and  $N = 79$  nuclei around  $^{132}\text{Sn}$ . A large scale shell model calculation has been performed which suggests the presence of configuration mixing in the structure of the excited levels in  $^{129}\text{Sn}$ .

## ACKNOWLEDGMENTS

The effort of the staffs of ILL is acknowledged for providing a good quality setup for the experiments. D.K. and T.B. gratefully acknowledge all kinds of support from VECC, DAE towards performing the experiment at an international laboratory.

- 
- [1] K. L. Jones *et al.*, *Nature (London)* **465**, 454 (2010).  
 [2] C. B. Hinke *et al.*, *Nature (London)* **486**, 341 (2012).  
 [3] R. Lica, H. Mach, L. M. Fraile, A. Gargano, M. J. G. Borge, N. Marginean, C. O. Sotty, V. Vedia, A. N. Andreyev, G. Benzoni *et al.*, *Phys. Rev. C* **93**, 044303 (2016).  
 [4] Ł. W. Iskra, R. Broda, R. V. F. Janssens, C. J. Chiara, M. P. Carpenter, B. Fornal, N. Hoteling, F. G. Kondev, W. Krolas, T. Lauritsen *et al.*, *Phys. Rev. C* **93**, 014303 (2016).  
 [5] <https://www.nndc.bnl.gov/ensdf>.  
 [6] L.-E. De Geer and G. B. Holm, *Phys. Rev. C* **22**, 2163 (1980).  
 [7] H. Gausemel, B. Fogelberg, T. Engeland, M. Hjorth-Jensen, P. Hoff, H. Mach, K. A. Mezilev, and J. P. Omtvedt, *Phys. Rev. C* **69**, 054307 (2004).  
 [8] J. A. Pinston, C. Foin, J. Genevey, R. Béraud, E. Chabanat, H. Faust, S. Oberstedt, and B. Weiss, *Phys. Rev. C* **61**, 024312 (2000).  
 [9] J. Genevey, J. A. Pinston, C. Foin, M. Rejmund, H. Faust, and B. Weiss, *Phys. Rev. C* **65**, 034322 (2002).  
 [10] R. L. Lozeva, G. S. Simpson, H. Grawe, G. Neyens, L. A. Atanasova, D. L. Balabanski, D. Bazzacco, F. Becker, P. Bednarczyk, G. Benzoni *et al.*, *Phys. Rev. C* **77**, 064313 (2008).  
 [11] E. Teruya, N. Yoshinaga, K. Higashiyama, and A. Odahara, *Phys. Rev. C* **92**, 034320 (2015).  
 [12] H.-K. Wang, K. Kaneko, Y. Sun, Y.-Q. He, S.-F. Li, and J. Li, *Phys. Rev. C* **95**, 011304(R) (2017).  
 [13] Z. W. Li, B. C. He, L. Li, Y. A. Luo, L. N. Bao, F. Pan, and J. P. Draayer, *Int. J. Mod. Phys. E* **31**, 2250014 (2022).  
 [14] J.-M. Régis, A. Esmaylzadeh, J. Jolie, V. Karayonchev, L. Knafla, U. Köster, Y. H. Kim, and E. Strub, *Nucl. Instrum. Methods Phys. Res. A* **955**, 163258 (2020).  
 [15] D. Kumar, T. Bhattacharjee, S. S. Alam, S. Basak, L. Gerhard, L. Knafla, A. Esmaylzadeh, M. Ley, F. Dunkel, K. Schomaker, J.-M. Régis, J. Jolie, Y. H. Kim, U. Köster, G. S. Simpson, and L. M. Fraile, *Phys. Rev. C* **106**, 034306 (2022).  
 [16] J.-M. Régis, N. Saed-Samii, M. Rudigier, S. Ansari, M. Dannhoff, A. Esmaylzadeh, C. Fransen, R.-B. Gerst, J. Jolie, V. Karayonchev, C. Müller-Gatermann, and S. Stegemann, *Nucl. Instrum. Methods Phys. Res. A* **823**, 72 (2016).  
 [17] F. H. Garcia, C. Andreoiu, G. C. Ball, N. Bernier, H. Bidaman, V. Bildstein, M. Bowry, D. S. Cross, M. R. Dunlop, R. Dunlop *et al.*, *Phys. Rev. C* **103**, 024310 (2021).  
 [18] Yu. Khazov, I. Mitropolsky, and A. Rodionov, *Nucl. Data Sheet* **107**, 2715 (2006).  
 [19] B. A. Brown and W. D. M. Rae, *Nucl. Data Sheets* **120**, 115 (2014).  
 [20] B. A. Brown, N. J. Stone, J. R. Stone, I. S. Towner, and M. Hjorth-Jensen, *Phys. Rev. C* **71**, 044317 (2005).  
 [21] J. Timar, Z. Elekes, and B. Singh, *Nucl. Data Sheets* **121**, 143 (2014).  
 [22] S. S. Alam, T. Bhattacharjee, D. Banerjee, A. Saha, S. Das, M. S. Sarkar, and S. Sarkar, *Phys. Rev. C* **99**, 014306 (2019).